DOI: 10.1002/ejic.200600764

A Series of Lithium Rare Earth Polyphosphates [$LiLn(PO_3)_4$] (Ln = La, Eu, Gd) and Their Structural, Optical, and Electronic Properties

Jing Zhu,[a] Wen-Dan Cheng,*[a] Dong-Sheng Wu,[a] Hao Zhang,[a] Ya-Jing Gong,[a] Hua-Nan Tong,[a] and Dan Zhao[a]

Keywords: Density functional calculations / UV/Vis spectroscopy / Rare earths / Phosphates

The structural, optical, and electronic properties of a series of lithium rare earth polyphosphates [$LiLn(PO_3)_4$] [Ln = La (**1**), Eu (**2**), Gd (**3**)] have been investigated by means of single-crystal X-ray diffraction, elemental analyses, and spectroscopic measurements, as well as calculations of energy-band structures, density of states, and optical response functions by density functional methods. These $LiLn(PO_3)_4$ systems are monoclinic with space group $C2/c$ and $Z = 4$. Their unit-cell parameters decrease as the ionic radius of Ln^{3+} decreases ($La^{3+} > Eu^{3+} > Gd^{3+}$). Both $(PO_4)^{3-}$ zig-zag chains and infinite chains formed by the alternate connection of LnO_8 polyhedra and LiO_4 tetrahedra run parallel to the *b*-axis in the structure. The energy-band structures, density of states, the chemical bonds, and optical properties have been investigated by density functional methods for some of the title compounds.

Introduction

Rare earth phosphate materials have been extensively investigated due to their structural diversity[1–3] and potential properties (magnetism,[4] electricity,[5] and optics[6]). Furthermore, their chemical and thermal stability ensures their utility in industrial applications. The common basic structural unit of these materials is the PO_4 group, and the varied condensations of PO_4 groups result in several structural families,[7–10] one of which is polyphosphates with the general formula [$MLn(PO_3)_4$] (M = alkali metal, Ln = rare earth metal).[11] Some polyphosphates with interesting optical properties have been reported in this family. For example, Yamada et al. have reported the use of [$LiNd(PO_3)_4$][12,13] as a solid-state laser material whose relatively large Nd–Nd distance gives rise to a lesser degree of fluorescence quenching. Parreu et al. have investigated noncentrosymmetric [$KLn(PO_3)_4$] (Ln = Nd, Gd) crystals[14,15] and explored their second harmonic generation, and Naili et al. have reported the crystal structures of [$MGd(PO_3)_4$] (M = K, Cs).[16,17] Recently, [$NaLa(PO_3)_4$][18] was synthesized in our laboratory. In addition, some phosphates involving lithium, such as [$LiMPO_4$] (M = Fe, Co, Ni),[19] exhibit excellent electrochemical properties with potential applications in lithium ion batteries. Although the lattice parameters of [$LiLn(PO_3)_4$] (Ln = La, Eu) have been reported previously,[20,21] no X-ray crystal structural determinations were able to support these parameters.

Here we will report the structures and optical properties of [$LiLn(PO_3)_4$] [Ln = La (**1**), Eu (**2**), Gd (**3**)]. We will also describe their electronic properties and the results of calculations of the crystal energy bands, density of states (DOS), and optical response functions of **1** and **3** by density functional methods in order to analyze the chemical bonding properties and electronic origins of the optical transitions.

Results and Discussion

Crystal Structure Descriptions

Crystals of **1**–**3** are isostructural and crystallize in the monoclinic space group $C2/c$ (see Supporting Information). The asymmetric units of **1**–**3** have the same number of crystallographically distinct atoms. As expected, the unit-cell parameters of **1**–**3** decrease as the ionic radius of Ln^{3+} decreases ($La^{3+} > Eu^{3+} > Gd^{3+}$). Selected bond lengths and angles are given in Table 1. The structure can be simply described as a three-dimensional framework made up from $(PO_4)^{3-}$ zig-zag chains and infinite chains involving LnO_8 and LiO_4 polyhedra. We will discuss their structural characterization by taking **1** as an example. Figure 1 shows a projection of the structure of **1** along the *b*-axis. The basic structural units are PO_4, LaO_8, and LiO_4 polyhedra. Two crystallographically distinct $P(1)O_4$ and $P(2)O_4$ tetrahedra form $(PO_4)^{3-}$ zig-zag chains by corner-sharing along the *b*-axis. The P(1) atom is connected to O(1), O(2), O(3), and O(4), and the P(2) atom is connected to O(2), O(3), O(5), and O(6). All P–O bond distances vary from 1.483(4) to

[a] State Key Laboratory of Structural Chemistry, Fujian Institute of Research on the Structure of Matter, Chinese Academy of Sciences,
Fuzhou, Fujian 350002, P. R. China
E-mail: cwd@fjirsm.ac.cn
Supporting information for this article is available on the WWW under http://www.eurjic.org or from the author.

Table 1. Selected bond lengths [Å] and angles [°] for compounds **1**–**3**.

			$[LiLa(PO_3)_4]$ (**1**)				
La–O6 (×2)	2.437(3)	P1–O1	1.491(4)	O1–P1–O4	118.6(2)	O6–P2–O5	119.5(2)
La–O1 (×2)	2.482(4)	P1–O4	1.500(3)	O1–P1–O2	106.4(2)	O6–P2–O3	111.8(2)
La–O5 (×2)	2.556(3)	P1–O2	1.592(4)	O4–P1–O2	111.5(2)	O5–P2–O3	106.9(2)
La–O4 (×2)	2.636(4)	P1–O3	1.595(3)	O1–P1–O3	111.4(2)	O6–P2–O2	110.0(2)
Li–O5 (×2)	1.945(8)	P2–O6	1.483(4)	O4–P1–O3	104.9(2)	O5–P2–O2	105.4(2)
Li–O4 (×2)	1.985(8)	P2–O5	1.492(3)	O2–P1–O3	103.1(2)	O3–P2–O2	101.5(2)
		P2–O3	1.594(3)				
		P2–O2	1.606(4)				
			$[LiEu(PO_3)_4]$ (**2**)				
Eu–O6 (×2)	2.333(3)	P1–O1	1.481(3)	O1–P1–O4	118.3(2)	O6–P2–O5	119.8(2)
Eu–O1 (×2)	2.388(4)	P1–O4	1.497(3)	O1–P1–O2	106.7(2)	O6–P2–O3	111.9(2)
Eu–O5 (×2)	2.452(3)	P1–O2	1.583(3)	O4–P1–O2	111.2(2)	O5–P2–O3	107.9(2)
Eu–O4 (×2)	2.540(3)	P1–O3	1.584(3)	O1–P1–O3	111.5(2)	O6–P2–O2	109.9(2)
Li–O5 (×2)	1.955(9)	P2–O6	1.481(3)	O4–P1–O3	105.1(2)	O5–P2–O2	104.6(2)
Li–O4 (×2)	1.975(8)	P2–O5	1.481(3)	O2–P1–O3	103.0(2)	O3–P2–O2	101.0(2)
		P2–O3	1.583(3)				
		P2–O2	1.601(3)				
			$[LiGd(PO_3)_4]$ (**3**)				
Gd–O6 (×2)	2.321(5)	P1–O1	1.485(5)	O1–P1–O4	118.5(3)	O6–P2–O5	119.7(3)
Gd–O1 (×2)	2.379(5)	P1–O4	1.496(5)	O1–P1–O2	106.0(3)	O6–P2–O3	112.1(3)
Gd–O5 (×2)	2.436(5)	P1–O2	1.584(5)	O4–P1–O2	111.4(3)	O5–P2–O3	107.6(3)
Gd–O4 (×2)	2.533(5)	P1–O3	1.595(5)	O1–P1–O3	111.7(3)	O6–P2–O2	110.0(3)
Li–O5 (×2)	1.97(1)	P2–O6	1.486(5)	O4–P1–O3	105.3(3)	O5–P2–O2	104.6(3)
Li–O4 (×2)	1.98(1)	P2–O5	1.490(5)	O2–P1–O3	102.9(3)	O3–P2–O2	101.1(3)
		P2–O3	1.578(5)				
		P2–O2	1.610(5)				

1.606(4) Å, and the O–P–O angles range from 101.5(2)° to 119.5(2)° (Table 1), thus indicating that these PO_4 tetrahedra are distorted. The largest distance is the P–O bond in the P–O–P bridge and the shortest one corresponds to that in the nonbridging connections. The $(PO_4)^{3-}$ chains are isolated from each other and surrounded by LaO_8 and LiO_4 polyhedra. In addition, an alternating arrangement of LaO_8 and LiO_4 polyhedra forms infinite chains along the *b*-axis by edge-sharing (Figure 2), each of which is surrounded by neighboring $(PO_4)^{3-}$ zig-zag chains. The La atom is coordinated by eight O atoms and the LaO_8 polyhedra are distorted, with La–O bond lengths ranging from 2.437(3) to 2.636(4) Å (Table 1). Each LaO_8 polyhedron is corner-connected to eight different PO_4 tetrahedra and edge-connected to two LiO_4 tetrahedra. The isolation of the LaO_8 polyhedra gives rise to large La–La distances, the shortest of which is 6.5690(3) Å. The Li atom is four-coordinate, with the Li–O bond distance ranging from 1.945(8) to 1.985(8) Å. Each LiO_4 tetrahedron shares all four O atoms with two LaO_8 polyhedra and four different PO_4 tetrahedra. The edge-sharing of LaO_8 and LiO_4 polyhedra results in infinite chains along the *b*-axis.

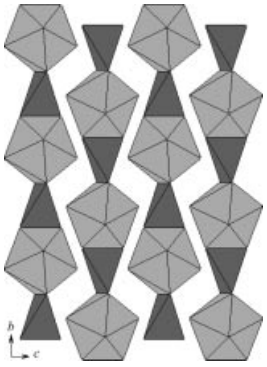

Figure 2. Projection of the structure of **1** along the *a*-axis showing the alternating arrangement of LaO_8 polyhedra and LiO_4 tetrahedra (the P atoms have been omitted for clarity).

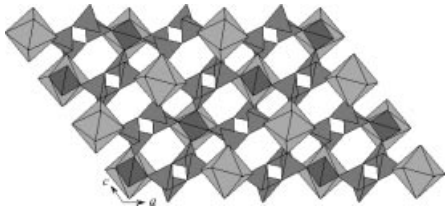

Figure 1. Projection of the structure of **1** along *b*-axis.

Band Structure, Density of States, and Chemical Bonds

The energy band structures and density of states (DOS) of **1** and **3** were calculated by density functional methods. For **3**, the spin-polarization was properly taken into account by considering the unpaired f-electron effect of the Gd^{3+} ion (α and β represent spin-up and spin-down, respectively). The calculated band structure of **1**, as shown in Fig-

ure 3, displays similar features, except for the f-band, to that of **3**, which is given as Supporting Information. In order to assign these bands, the total density of states (TDOS) and partial DOS (PDOS) of **1** and **3** are shown in Figure 4.

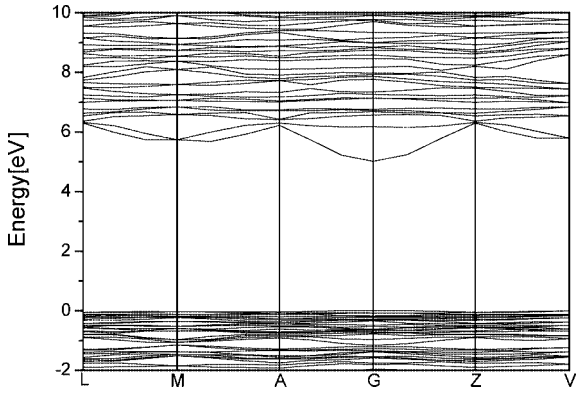

Figure 3. Calculated band structure of **1**.

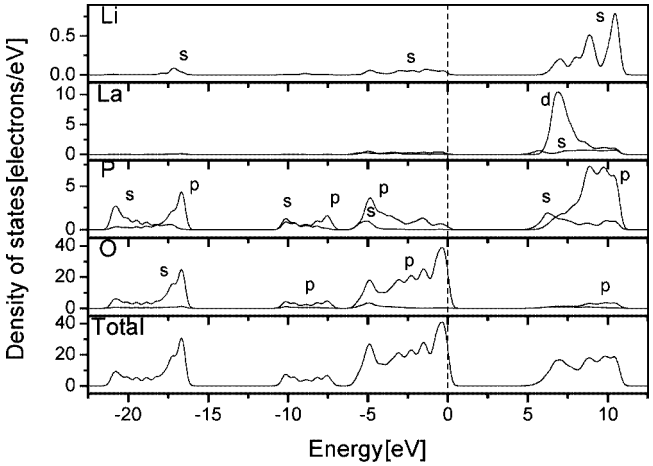

(a)

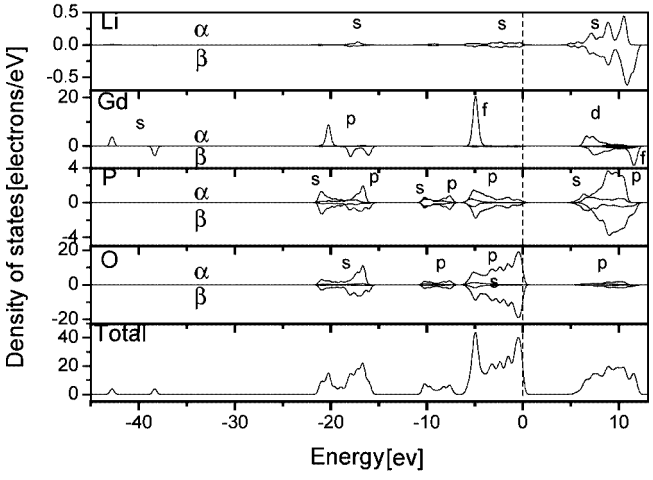

(b)

Figure 4. Total and partial densities of states of **1** (a) and **3** (b).

The calculated band structures of **1** and **3** exhibit similar features. It is observed that the top of the valence bands (VBs) is nearly flat and close to the Fermi level (0.0 eV), and the bottom of the conduction bands (CBs) exhibits obvious dispersion. The lowest energy of the CBs is localized at G (Figure 3), which means that **1** and **3** show an insulator character with a direct bandgap of around 5.02 and 4.99 eV, respectively. According to Figure 4, the O 2p states are the main contributors to the VBs ranging from –10.7 eV to the Fermi level, and the O 2s states form the VBs between –21.5 and –16.0 eV. In addition, the CBs between 5.0 and 11.0 eV are mostly formed by the P 3p states. The La 5d and Gd 5d states also give rise to CBs in **1** and **3**, respectively. Furthermore, for **3**, the VBs near about –40.0, –20.0, and –5.0 eV also result from the Gd 5s, Gd 5p, and Gd 4f states, respectively.

We also elucidated the features of the chemical bonds for **1** and **3** on the basis of the total and angular momentum projected DOS (Figure 4). In the range from –10.7 eV to the Fermi level the O 2p and P 3p states exist simultaneously, although the DOS is much larger for the former, which indicates that some P 3p electrons transform into the VBs and take part in the covalent interactions between P and O atoms and that hybridization between the P 3p and O 2p states takes place. The chemical bonding properties were also confirmed by means of the population analysis. The calculated bond orders of **1** and **3** in the unit cell are 0.45–0.82, 0.20–0.30, and 0.02–0.03 e for P–O, Ln–O, and Li–O bonds, respectively. It is well known that a covalent single-bond order is generally 1.0 e. Accordingly, the covalent character of the P–O bond is larger than that of the Ln–O bond, and the ionic character of the Li–O bond is larger than that of the Ln–O bond.

Optical Properties

Figure 5 illustrates the absorption and emission spectra of **1**–**3**. The absorption spectra were determined by the diffuse-reflectance technique. $F(R)$ and R are linked by $F(R) = (1 - R)^2/2R$, where R is the reflectance and $F(R)$ is the Kubelka–Munk remission function. The minima in the second-derivative curves of the Kubelka–Munk function are taken as the position of the absorption bands. Their absorption edges are around 320 (3.88), 330 (3.76), and 350 nm (3.55 eV), respectively. A strong absorption peak only appears at around 245 nm (5.07 eV) for **1**, 250 nm (4.97 eV) for **2**, and 260 nm (4.78 eV) for **3**.

In order to assign these experimental spectra, we examined the linear optical response properties of crystals **1** and **3**. We calculate the imaginary part $\varepsilon_2(\omega)$ and the real part $\varepsilon_1(\omega)$ of the frequency-dependent dielectric function without the DFT scissor-operator approximation, as displayed in Figure 6. The $\varepsilon_2(\omega)$ part can be used to describe the real transitions between the occupied and unoccupied electronic states. There are distinct peaks at around 7.50 and 8.50 eV for **1** and **3**, respectively, which correspond to those of the experimental spectra [Figure 5(a)]. According to Figure 4,

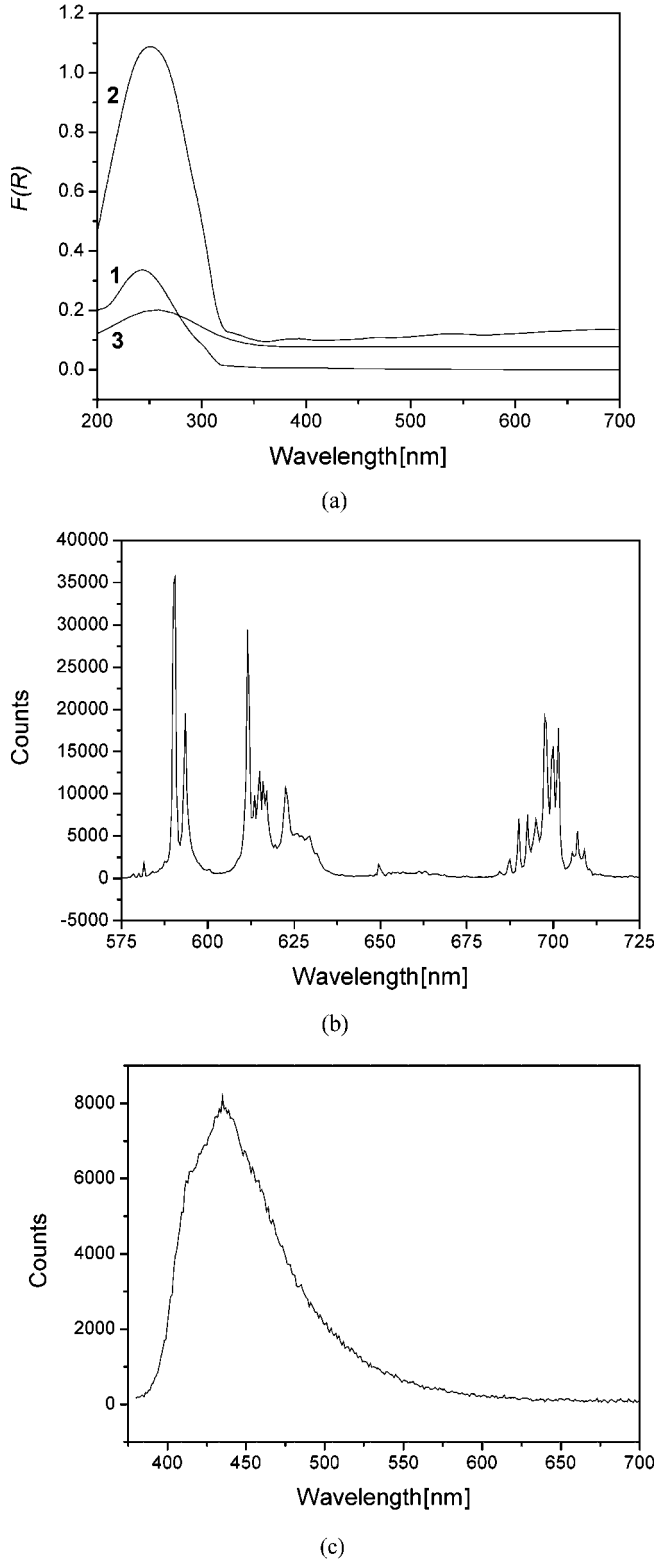

Figure 5. Absorption spectra of **1**–**3** (a); emission spectrum of **2** upon excitation at 295 nm (b); emission spectrum of **3** upon excitation at 365 nm (c).

these peaks are due to the electronic transitions from the O 2p to La 5d states for **1** and from the O 2p to Gd 5d states for **3**. In addition, comparing the calculated UV/Vis absorption edges (about 5.20 eV for **1** and 4.60 eV for **3**) of the crystals with the experimental ones (about 3.88 eV for **1** and 3.55 eV for **3**) of the powder samples shows that the transmission width is larger for the crystals than the powder samples, which indicates that the result of the calculation is reasonable. For **3**, the emission peak is located at 435 nm (2.86 eV) at an excitation wavelength of 365 nm [Figure 5(c)]. The emission energy is less than the experimental absorption edge of 3.55 eV, which means that the emission peak probably originates from defects or excitons. For **2**, the emission spectrum displays the characteristic yellow-red emissions that result from the intraconfigurational electronic $^5D_0$–^7F_J transitions (J = 0–4) of the Eu^{3+} ion[22] in the range from 575 to 725 nm under excitation at 295 nm [Figure 5(b)]. Five emission regions correspond to 582 ($^5D_0$–$^7F_0$), 590–595 ($^5D_0$–$^7F_1$), 610–630 ($^5D_0$–$^7F_2$), 650 ($^5D_0$–$^7F_3$), and 685–710 nm ($^5D_0$–$^7F_4$), respectively. The presence of only one narrow band for the $^5D_0$–$^7F_0$ transition of the Eu^{3+} ion implies that there is only one such

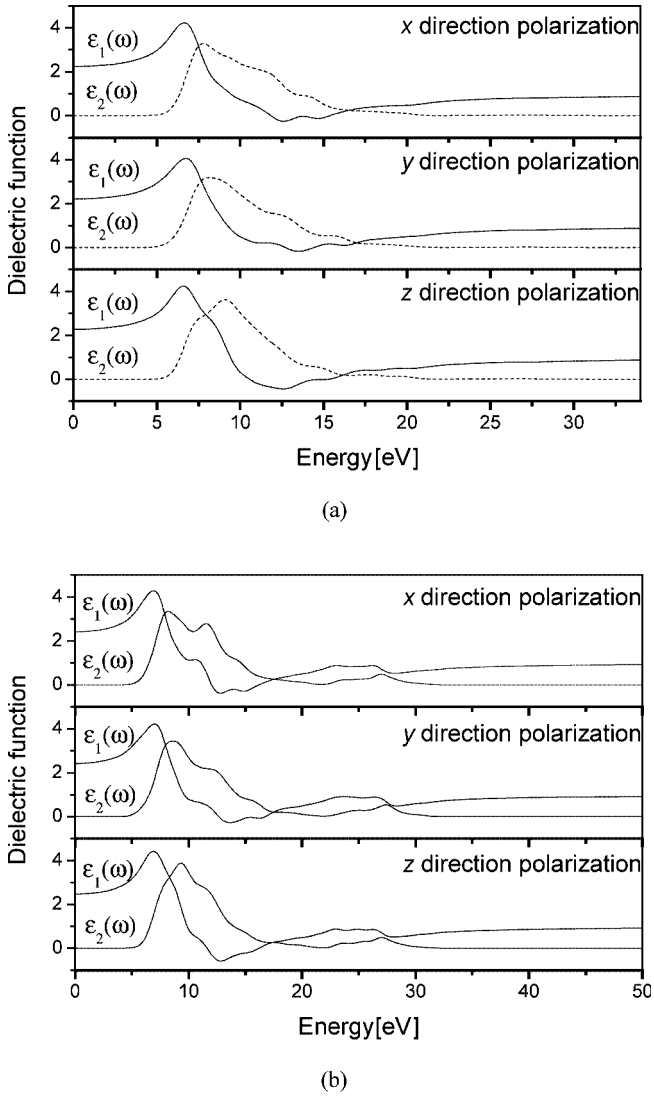

Figure 6. Calculated real and imaginary parts of the dielectric functions in different polarization directions for **1** (a) and **3** (b).

coordination environment, which is consistent with the above-mentioned structural data for **2**.

We also investigated the calculated dielectric constants of the static case, $\varepsilon(0)$, and the refractive indices, n, of **1** and **3**. The refractive index is linked to the dielectric constant by the relation $n^2(\omega) = \varepsilon(\omega)$. The calculated dielectric constants of the static case in the x, y, and z directions are 2.2378, 2.2135, and 2.2768 for **1** and 2.4142, 2.4232, and 2.4645 for **3**, respectively. The corresponding refractive indices in the different directions at 1064 nm are 1.5034, 1.4951, and 1.5165 for **1** and 1.5614, 1.5645, and 1.5775 for **3**. It should be noted that the calculated dielectric constants of the static case and refractive indices at 1064 nm are larger for **3** than for **1**. Since the refractive indices of **1** and **3** have not been measured or reported, we compared the calculated results with the observed refractive indices of the other phosphate crystals, which generally range from 1.40 to 1.6;[23] the calculated refractive indices of **1** and **3** are therefore reasonable.

Conclusions

In summary, a series of isostructural lithium rare earth polyphosphates [LiLn(PO$_3$)$_4$] (Ln = La, Eu, Gd) have been synthesized by a high-temperature solution reaction. Their crystallographic data obtained by single-crystal X-ray diffraction show that their structures belong to the monoclinic space group $C2/c$. The unit-cell parameters of **1**–**3** decrease as the ionic radius of Ln^{3+} decreases ($La^{3+} > Eu^{3+} > Gd^{3+}$). Both $(PO_4)^{3-}$ zig-zag chains and infinite chains with an alternating arrangement of LaO_8 and LiO_4 polyhedra run along the b-axis. The Li–O bond exhibits ionic character, and the P–O bond is more covalent than the Ln–O bond. Spectral measurements and theoretical computations show that **1**–**3** are insulators. [LiEu(PO$_3$)$_4$] displays the characteristic yellow-red emissions that result from the intraconfigurational electronic $^5D_0$–^7F_J transitions (J = 0–4) of the Eu^{3+} ion. In addition, the dielectric constants of the static case, $\varepsilon(0)$, and refractive indices, n, of [LiLa(PO$_3$)$_4$] and LiGd(PO$_3$)$_4$ have also been estimated. Further studies aimed at synthesizing new phosphate materials with other alkali and rare earth metals are currently in progress.

Experimental Section

Syntheses: Single crystals of **1**–**3** were prepared by a high-temperature solution reaction from Li_2CO_3, La_2O_3 (**1**), Eu_2O_3 (**2**), or Gd_2O_3 (**3**), and $NH_4H_2PO_4$ with an Li/Ln/P molar ratio of 7:1:12. The excess Li_2CO_3 and $NH_4H_2PO_4$ formed the flux. The starting mixtures were finely ground in an agate mortar to ensure the best homogeneity and reactivity, then placed in a platinum crucible and heated at 473 K for 4 h. The mixtures were then reground and heated to 1173 K for 24 h. Finally, the mixture was cooled to 773 K at a rate of 2 K h^{-1}, followed by air-quenching to room temperature. A few colorless, block-shaped crystals were obtained from the melt of the mixtures.

Crystal Structure Determinations: Single crystals of **1**–**3** with dimensions $0.18 \times 0.10 \times 0.03$ (**1**), $0.20 \times 0.04 \times 0.02$ (**2**), and $0.30 \times 0.12 \times 0.08$ mm (**3**) were selected for X-ray diffraction determination. The diffraction data for **1** were collected with a Siemens SMART CCD diffractometer with graphite-monochromated Mo-K_a radiation (λ = 0.71073 Å) using the $\omega/2\theta$-scan mode at a temperature of 293 K, and those for **2** and **3** were collected with a Rigaku Mercury CCD diffractometer with graphite-monochromated Mo-K_a radiation (λ = 0.71073 Å) using the ω-scan mode at a temperature of 293 K. Lorentz and polarization corrections were applied to all data. The structures were solved by direct methods and refined on F^2 by the full-matrix least-squares method with SHELXL97.[24] The positions of the La, Eu, and Gd atoms were refined by direct methods and the remaining atoms were located in successive difference Fourier syntheses. In order to confirm the chemical compositions of the four compounds, the single crystals of **1**–**3** investigated with the diffractometer were analyzed by energy-dispersive X-ray spectroscopy (EDX) using a JSM6700F scanning electron microscope. The obtained results are in good agreement with those obtained by the refinement of the crystal structures. No impurity elements were detected, although the light element Li could not be satisfactorily determined by the EDX measurement. The results of the elemental analyses are given as Supporting Information. Crystal data for **1**: LiLa(PO$_3$)$_4$ (461.73), monoclinic, space group $C2/c$, T = 293(2) K, a = 16.6230(3), b = 7.1198(1), c = 9.905 Å, β = 126.43°, V = 943.19(2) Å^3, Z = 4, $D_{calcd.}$ = 3.252 g cm^{-3}, $F(000)$ = 864, μ(Mo-K_a) = 5.272 mm^{-1}, 2461 reflections collected, 891 unique (R_{int} = 0.0335), R_1 = 0.0282, wR_2 = 0.0685 [$I > 2\sigma(I)$], R_1 = 0.0284, wR_2 = 0.0686 (all data) and final Gof = 1.017. Crystal data for **2**: LiEu(PO$_3$)$_4$ (474.78), monoclinic, space group $C2/c$, T = 293(2) K, a = 16.3300(9), b = 7.0330(4), c = 9.6465(6) Å, β = 126.14(3)°, V = 894.7(0) Å^3, Z = 4, $D_{calcd.}$ = 3.525 g cm^{-3}, $F(000)$ = 888, μ(Mo-K_a) = 7.794 mm^{-1}, 3389 reflections collected, 1032 unique (R_{int} = 0.0412), R_1 = 0.0259, wR_2 = 0.0584 [$I > 2\sigma(I)$], R_1 = 0.0279, wR_2 = 0.0596 (all data) and final Gof = 1.000. Crystal data for **3**: LiGd(PO$_3$)$_4$ (480.07), monoclinic, space group $C2/c$, T = 293(2) K, a = 16.330(1), b = 7.0327(4), c = 9.6450(8) Å, β = 126.12(4)°, V = 894.8(1) Å^3, Z = 4, $D_{calcd.}$ = 3.564 g cm^{-3}, $F(000)$ = 892, μ(Mo-K_a) = 8.195 mm^{-1}, 3313 reflections collected, 1030 unique (R_{int} = 0.0426), R_1 = 0.0319, wR_2 = 0.0820 [$I > 2\sigma(I)$], R_1 = 0.0323, wR_2 = 0.0822 (all data) and final Gof = 1.025. Further details of the crystal-structure investigations may be obtained from the Fachinformationzentrum Karlsruhe, 76344 Eggenstein-Leopoldshafen, Germany, on quoting the depository numbers CSD-416877 to -416879 (for **1**–**3**, respectively).

Spectral Measurements: The purity of the polycrystalline samples for spectral measurements of **1**–**3** was confirmed by powder XRD studies using a Rigaku DMAX2500 diffractometer with Cu-K_a radiation (step size of 0.05° and 2θ range of 10–80°). The powder XRD patterns of **1**–**3** are given as Supporting Information. The absorption spectra were recorded with a Lambda-35 UV/Vis spectrophotometer in the wavelength range 200–800 nm. The emission spectra were measured with an FLS920 time-resolved fluorescence spectrometer using an Xe lamp at room temperature.

Computational Details: The crystallographic data of **1** and **3** determined by single-crystal X-ray diffraction were used to calculate their electronic band structures. Calculations of electronic band structures were performed at the density functional theory (DFT) level using one of the three nonlocal gradient-corrected exchange-correlation functionals (GGA-PBE) and with the CASTEP code,[25,26] which uses a plane wave basis set for the valence electrons and norm-conserving pseudopotential[27] for the core states. The number of plane waves included in the basis was determined by a cutoff energy, E_c, of 550 eV. Pseudoatomic calculations were performed for O ($2s^2 2p^4$), P ($3s^2 3p^3$), Li ($2s^1$), La ($5d^1 6s^2$), and

Gd ($4f^7 5s^2 5p^6 5d^1 6s^2$). The calculating parameters and convergent criteria were set by the default values of the CASTEP code.[25] The linear optical properties were also calculated; $\varepsilon_2(\omega)$ can be thought of as detailing the real transitions between occupied and unoccupied electronic states. Since the dielectric constant describes a causal response, the real and imaginary parts are linked by the Kramers–Kronig transformation,[28] where P is the principal value of the integral. This transformation is used to obtain the real part of the dielectric function, $\varepsilon_1(\omega)$.

$$\varepsilon_1(\omega) - 1 = \frac{2}{\pi} \mathrm{P} \int_0^\infty \frac{\omega' \varepsilon_2(\omega') d\omega'}{\omega'^2 - \omega^2} \quad \text{and} \quad \varepsilon_2(\omega) = -\frac{2\omega}{\pi} \mathrm{P} \int_0^\infty \frac{\varepsilon_1(\omega') d\omega'}{\omega'^2 - \omega^2}$$

Supporting Information (see footnote on the first page of this article): Full results of elemental analysis for **1**–**3**. Experimental and simulated X-ray powder diffraction patterns of **1**–**3**. The calculated band structure of **3**.

Acknowledgments

This investigation was supported by the National Basic Research Program of China (grant no. 2004CB720605), the National Natural Science Foundation of China under projects 20373073 and 90201015, the Science Foundation of the Fujian Province (grant no. E0210028), and the Foundation of the State Key Laboratory of Structural Chemistry (grant no. 060007).

[1] L. Campayo, F. Audubert, D. Bermache-Assollant, *Solid State Ionics* **2005**, *176*, 2663–2669.
[2] L. Rghioui, L. E. Ammari, L. Benarafa, J. P. Wignacourt, *Acta Crystallogr., Sect. C* **2002**, *58*, i90–i91.
[3] I. Szczygiel, *Solid State Sci.* **2005**, *7*, 189–194.
[4] J. M. Cole, M. R. Lees, J. A. K. Howard, R. J. Newport, G. A. Saunders, E. Schönherr, *J. Solid State Chem.* **2000**, *150*, 377–382.
[5] M. Ferid, K. Horchani-Naifer, *Solid State Ionics* **2005**, *176*, 1949–1953.
[6] J. J. Gavaldà, I. Parreu, R. Solé, X. Solans, F. Díaz, M. Aguiló, *Chem. Mater.* **2005**, *17*, 6746–6754.
[7] A. Hamady, T. Jouini, *Acta Crystallogr., Sect. C* **1996**, *52*, 2949–2951.
[8] H. Y.-P. Hong, S. R. Chinn, *Mater. Res. Bull.* **1976**, *11*, 421–428.
[9] W. Rekik, H. Naïli, T. Mhiri, *Acta Crystallogr., Sect. C* **2004**, *60*, i50–i52.
[10] I. Szczygiel, *Thermochim. Acta* **2004**, *417*, 75–78.
[11] E. B. Zarkouna, A. Driss, *Acta Crystallogr., Sect. E* **2004**, *60*, i102–i104.
[12] T. Yamada, K. Otsuka, J. Nakano, *J. Appl. Phys.* **1974**, *45*, 5096.
[13] K. Otsuka, T. Yamada, *Appl. Phys. Lett.* **1975**, *26*, 311.
[14] I. Parreu, J. J. Carvajal, X. Solans, F. Díaz, M. Aguiló, *Chem. Mater.* **2006**, *18*, 221–228.
[15] I. Parreu, R. Solé, J. Gavaldà, J. Massons, F. Díaz, M. Aguiló, *Chem. Mater.* **2003**, *15*, 5059–5064.
[16] H. Naïli, T. Mhiri, *Acta Crystallogr., Sect. E* **2005**, *61*, i204–i207.
[17] H. Ettis, H. Naïli, T. Mhiri, *Cryst. Growth Des.* **2003**, *3*, 599–602.
[18] J. Zhu, W. D. Cheng, D. S. Wu, H. Zhang, Y. J. Gong, H. N. Tong, *J. Solid State Chem.* **2006**, *179*, 597–604.
[19] R. Ruffo, R. A. Huggins, C. M. Mari, M. Piana, W. Weppner, *Ionics* **2005**, *11*, 213–219.
[20] N. N. Chudinova, N. V. Vinogradova, *Izv. Akad. Nauk SSSR, Neorg. Mater.* **1979**, *15*, 2171–2175; *Chem. Abstr.* **1980**, *92*, 100210m.
[21] M. F. Moktar, N. Kbir-Ariguib, M. Trabelsi, *J. Solid State Chem.* **1981**, *38*, 130–132.
[22] E. E. S. Teotonio, H. F. Brito, M. C. F. C. Felinto, L. C. Thompson, V. G. Young, O. L. Malta, *J. Mol. Struct.* **2005**, *751*, 85–94.
[23] *Lange's Handbook of Chemistry*, 13th ed. (Ed.: J. A. Deans), McGraw–Hill Book Company, New York, **1985**.
[24] G. M. Sheldrick, *SHELXTL-97, Program for Refining Crystal Structure*, University of Göttingen, Germany, **1997**.
[25] M. Segall, P. Linda, M. Probert, C. Pickard, P. Hasnip, S. Clark, M. Payne, *Materials Studio CASTEP*, version 2.2, **2002**.
[26] M. Segall, P. Linda, M. Probert, C. Pickard, P. Hasnip, S. Clark, M. Payne, *J. Phys.: Condens. Mater.* **2002**, *14*, 2717–2744.
[27] D. R. Hamann, M. Schluter, C. Chiang, *Phys. Rev. Lett.* **1979**, *43*, 1494–1497.
[28] J. R. Macdonald, M. K. Brachman, *Rev. Mod. Phys.* **1956**, *28*, 383.

Received: August 17, 2006
Published Online: November 6, 2006

